Technical Paper

Session: 7 - 4

Session Name: Bearing and Seals

Unified Prediction of Hydrodynamic Forces in Plain Annular Seals and Journal Bearings by means of an Analytically Derived Design Tool

Authors:

Sebastian Lang, Peter F. Pelz

Contact:

Prof. Dr.-Ing. Peter F. Pelz,
TU Darmstadt
Institut für Fluidsystemtechnik FST
Otto-Berndt-Straße 2
64287 Darmstadt
GERMANY

Phone: +49 6151 16 27100
Telefax: +49 6151 16 27110
E-Mail: peter.pelz@fst.tu-darmstadt.de

Summary

Annular seals and journal bearings are essential parts of rotating machinery and share comparable geometries characterized by narrow annuli between rotor and stator. Both machine elements exert hydrodynamic forces on the rotor that must not be neglected during the design process. Accurate prediction of these forces by means of fast and reliable design tools is required to optimize the rotordynamic shaft design within short time.

The paper deals with the analytical development of a unified design tool to predict the hydrodynamic forces for both annular seals and hydrodynamic bearings in rotating machinery. The requirements on such a unified tool are discussed in terms of various flow regimes that are to be expected in thin film flows in rotating machinery. Following that, the analytic derivation of our 'Clearance-Averaged Pressure Model' (CAPM) is described. All simplifications applied can be justified by means of the characteristic geometries of the narrow annuli. Especially, no further assumptions regarding the flow regime (laminar/turbulent), the role of fluid inertia or the friction modeling were applied. The CAPM provides a clear interface to the vast knowledge about friction modeling that has been accumulated in hydrodynamic lubrication research. Thus, the CAPM serves as a generalized modeling framework for all typical thin film flows in rotating machinery and includes both Reynolds' differential equation and the bulk-flow model as special cases. Hence, user-specific uncertainties on the applicability of a specific design tool for a specific application are reduced.

The accuracy of the current state of our model is assessed by means of comparisons to Computational Fluid Dynamics (CFD) results. We applied both the CAPM and CFD to test cases typically representing geometrical and operational characteristics of annular seals within a parameter study. The predicted hydrodynamic radial forces agreed well for all operating points considered. In contrast to that, the predicted tangential forces agreed well only if the flow number ϕ is small or if the preswirl is close to $\Gamma=0.5$. The observed differences are discussed by means of the different roles of velocity profile development throughout the annulus.

1. Introduction

Annular seals as well as journal bearings are essential components of rotating machinery like rotordynamic pumps. Both machine elements are characterized by narrow clearances between rotor and stator and the thin fluid films inside the annular fluid domains exert hydrodynamic forces on the rotor that must not be neglected during the rotordynamic design of the shaft. For the rotordynamic analyses during this design process, it is common practice to represent the rotordynamic influence of seals and bearings by means of direct and cross-coupled stiffness $\tilde{K}$ and $\tilde{k}$, direct and cross-coupled damping $\tilde{C}$ and $\tilde{c}$ and direct and cross-coupled inertia or mass $\tilde{M}$ and $\tilde{m}$ coefficients, see Fig. *1*. Note that in our notation throughout the paper, superscripts $\sim$ denote dimensional symbols.

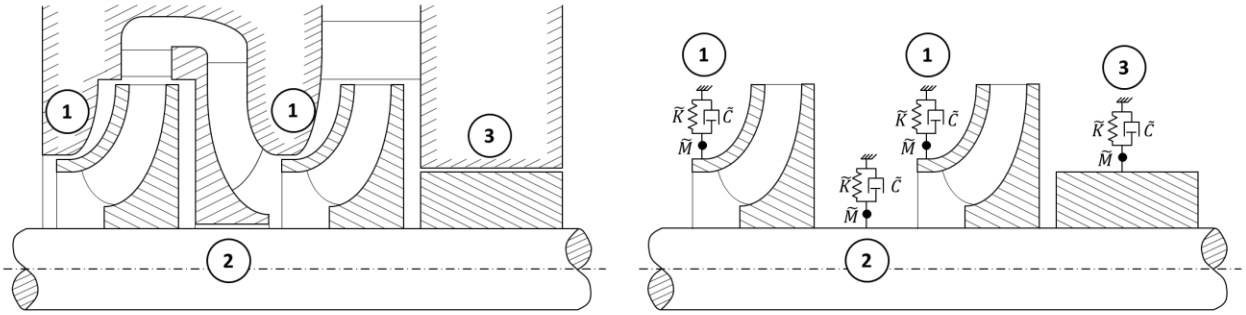

Figure 1: Annular seals inside a rotordynamic pump and their rotordynamic representation.

The rotordynamic coefficients are usually determined by means of a linear relationship

$$-\begin{bmatrix}\tilde{F}_x\\ \tilde{F}_y\end{bmatrix} = \begin{bmatrix}\tilde{K} & \tilde{k}\\ -\tilde{k} & \tilde{K}\end{bmatrix}\begin{bmatrix}\tilde{x}\\ \tilde{y}\end{bmatrix} + \begin{bmatrix}\tilde{C} & \tilde{c}\\ -\tilde{c} & \tilde{C}\end{bmatrix}\begin{bmatrix}\dot{\tilde{x}}\\ \dot{\tilde{y}}\end{bmatrix} + \begin{bmatrix}\tilde{M} & \tilde{m}\\ -\tilde{m} & \tilde{M}\end{bmatrix}\begin{bmatrix}\ddot{\tilde{x}}\\ \ddot{\tilde{y}}\end{bmatrix} \quad (1)$$

between the hydrodynamic forces $\tilde{F}_x$ and $\tilde{F}_y$ exerted on the shaft and the shaft's excitation $\tilde{x}$ and $\tilde{y}$ and their temporal derivatives, respectively [1]. Depending on the character of the shaft's excitation and movements, the coefficients in Eqn. 1 can become nonlinear or the matrices can lose their skew symmetry [2]. Furthermore, especially in case of long seals or bearings, additional torque coefficients need to be considered in Equ. 1. Nevertheless, independent of the exact form of Equ. 1, an accurate prediction of the hydrodynamic forces (and torques) for given shaft excitations (and inclinations) and movements is required to achieve reliable rotordynamic characterizations of seals and bearings. The determination of the hydrodynamic forces can be carried out experimentally or by means of numerical solution of the 3D Navier-Stokes equations (Computational Fluid Dynamics, CFD). But the high effort necessary to conduct both types of investigations is unacceptable during the design stage of a shaft. At this stage, fast and reliable design tools are required to efficiently predict the hydrodynamic forces and enable an optimization of the rotordynamic design within short time.

Annular seals and journal bearings share very comparable geometries characterized by narrow annuli between rotor and stator. Hydrostatic and hybrid journal bearings are bearings where the load capacity is primarily or at least partially provided by a high pressure drop across the bearing [3]. Process fluid bearings use the primary (often low viscosity, i.e. water) process medium as lubricant and often utilize a driving pressure difference that is already available in the process, i.e. the pump head of a rotordynamic pump stage. The former explanations indicate that there is a somewhat 'continuous' transition from annular seals to journal bearings or vice versa in rotating machinery like rotordynamic pumps. Furthermore, the impact on the rotordynamic

design of all these thin film fluid flows is represented in the same way via rotordynamic coefficients as given in Equ. 1.

In contrast, today's fast design tools for thin film flows in rotating machinery do not reflect the continuous transition from pure hydrodynamic journal bearing to pure annular seal application. Expert knowledge on the flow phenomena relevant in a specific application and flow features modeled in the respective design tools is required to assess their applicability for the given flow situation and operating conditions. Journal bearings are usually treated by means of Reynolds' differential equation. In the derivation of the basic form of this equation, firstly fluid inertia is neglected in comparison to viscous forces and secondly laminar velocity profiles are applied [3]. The corresponding approach in the field of annular seals is usually referenced to as 'bulk-flow' model. This approach formulates mass and momentum conservation for clearance-averaged velocities while neglecting shear stresses inside the fluid [5].

In addition to such user-specific applicability uncertainties, the model uncertainties themselves need to be added to the final prediction uncertainties, of course. Consequently, high security factors need to be applied in today's rotordynamic design. The objective of our work is to predict the hydrodynamic forces and rotordynamic coefficients of thin film flows in rotordynamic pumps within a unified design tool. Such a common approach is supposed to be inherently able to consider the flow phenomena relevant in pure hydrodynamic journal bearings and annular seals but also in the flow regimes in between these basic types. We think that the high security factors required with today's design tools can be reduced with such a unified tool as the user-specific applicability uncertainties will vanish.

We start our work by identifying the requirements on such a unified design tool and the state of the art related to these requirements. Following that, we describe the analytic approach and the numerical solution technique behind the current state of our design tool. We performed CFD simulations in order to assess the quality of our design tool's predictions already in a stage of the development when the planned test bench is not available yet. Finally, we apply our design tool and the CFD approach to test cases with geometrical and operational conditions typical for plain annular seal applications and compare the hydrodynamic forces predicted by both approaches.

2. Requirements and State of the Art

It is beneficial to start by going one step backwards and identify common assumptions behind Reynolds' differential equation and the bulk-flow model that can serve as basis for a unified modeling approach as well as individual assumptions that prevent these models from being universally applicable. Our intention is to create a modeling framework all the developments in the field of hydrodynamic lubrication theory can easily be adapted to. Ideally, the modeling framework should include Reynolds' differential equation and the bulk-flow model as special cases.

General Simplifications for Thin Film Flows

Though Reynolds' differential equation and the bulk-flow model originate from completely different flow regimes, both rely on the common assumption that a clearance-averaged pressure formulation is sufficient to characterize the hydrodynamic forces acting on the rotor. Indeed, an order of magnitudes analysis of the differential forms of continuity equation and radial momentum balance inside the annulus yield

$$\frac{\partial p}{\partial y} \lesssim \mathcal{O}(\psi) \tag{2}$$

where $p \coloneqq 2\tilde{p}/\left(\tilde{\varrho}\tilde{\Omega}^2\tilde{R}^2\right)$ is the dimensionless pressure, $\tilde{\Omega}\tilde{R}$ is the circumferential velocity of the shaft surface, $y \coloneqq \tilde{y}/\tilde{h}$ is the dimensionless channel coordinate in radial direction and $\psi \coloneqq \tilde{\bar{h}}/\tilde{R}$ is the relative mean clearance. Note that typical values of $\psi \ll \mathcal{O}(1)$ are a fundamental and common geometrical feature of all thin film flows in rotating machinery. Thus, an analytic approach relying on a clearance-averaged pressure formulation should provide the basis for a unified model. Accordingly, we denote our unified modeling approach as 'Clearance-Averaged Pressure Model' (CAPM).

Assumptions Specific to Individual Flow Regimes

The flow regimes we have to distinguish are related to the role of fluid inertia in the film flow. Different treatments of fluid inertia change the nature of the governing equations in a fundamental way. Thus, models specialized to single inertia regimes can not serve as basis for a universal approach.

Kahlert [7] was one of the first to realize that the role of fluid inertia for the prediction of the hydrodynamic forces in a hydrodynamic journal bearing changes dramatically as the relation

$$Re_\varphi^* \coloneqq \frac{\psi\tilde{\varrho}\tilde{\Omega}^2\tilde{R}^2/\tilde{\bar{h}}}{\tilde{\mu}\tilde{\Omega}\tilde{R}/\tilde{\bar{h}}^2} = \psi Re_\varphi \qquad \left(\triangleq \frac{\text{convective terms}}{\text{viscous terms}}\right) \tag{3}$$

changes its order of magnitude, where $Re_\varphi \coloneqq \tilde{\Omega}\tilde{R}\tilde{\bar{h}}/\tilde{\nu}$ is the circumferential Reynolds number. We denote Re_φ^* 'circumferential film Reynolds number' in the following. Based on Re_φ^*, two inertia regimes can be distinguished: If $Re_\varphi^* \ll \mathcal{O}(1)$, fluid inertia is negligible in comparison to viscous forces and friction exerted by the channel walls, respectively. In this inertia regime, Reynolds' differential equation accurately approximates the thin film flow, see i.e. [3]. As the circumferential film Reynolds number approaches unity, i.e. $Re_\varphi^* \sim \mathcal{O}(1)$, convective terms need to be considered in the governing equations and several authors have done so, see i.e. [8]-[12]. In case of both inertia regimes $Re_\varphi^* \ll \mathcal{O}(1)$ and $Re_\varphi^* \sim \mathcal{O}(1)$, fully developed velocity profiles are used to evaluate the mass and momentum balances for the thin film flow. This can be done for both laminar flow as well as turbulent flow conditions, see i.e. the two complementary papers of Launder and Leschziner [10]. But the assumption of fully established velocity profiles corresponds to the assumption of a negligible effect of fluid inertia on the velocity profiles. Consequently, further discussion on the requirements for this assumption is necessary.

It was Elrod [12] who reinterpreted Kahlert's [7] inertia parameter of Eqn. 3 in a very intuitive way for a slider bearing: In his words, the inertia parameter represents a dimensionless diffusion time, i.e. it relates the typical time scales shear waves need to travel through the fluid domain $\tilde{\bar{h}}^2/\tilde{\nu}$ to a typical transit time of the fluid through the bearing. In case of externally pressurized thin film flows, the typical transit time through the annulus is related to the mean axial flow velocity $\tilde{\bar{C}}_z$ and the bearing's width or seal's length $\tilde{L}$, respectively. Hence, we receive an axial film Reynolds number

$$Re_z^* \coloneqq \frac{\tilde{\bar{h}}^2/\tilde{\nu}}{\tilde{L}/\tilde{\bar{C}}_z} = \frac{\psi Re_z}{L} = \frac{\phi}{L}\psi Re_\varphi \qquad \left(\triangleq \frac{\text{diffusion time}}{\text{transit time}}\right) \tag{4}$$

as second 'inertia parameter' in externally pressurized bearings and seals. In Eqn. 4, $Re_z \coloneqq \tilde{\bar{C}}_z\tilde{\bar{h}}/\tilde{\nu}$ denotes the axial Reynolds number, $\phi \coloneqq Re_z/Re_\varphi = \tilde{\bar{C}}_z/\left(\tilde{\Omega}\tilde{R}\right)$ denotes the flow number and $L \coloneqq \tilde{L}/\tilde{R}$ denotes the dimensionless bearing width or seal length, respectively. If $Re_z^* \ll \mathcal{O}(1)$, the velocity profiles in the thin film flow reach a fully developed state very close to the annulus' inlet and this assumption of all the references cited for the inertia regimes $Re_\varphi^* \ll \mathcal{O}(1)$

and $Re_{\varphi}^{*} \sim \mathcal{O}(1)$ above holds. On the contrary, if $Re_{\varphi}^{*} \gg \mathcal{O}(1)$, the transit time of the fluid through the annulus is too short to enable any significant development of velocity profiles. Hence, potential flow profiles can be utilized throughout the annulus as it is done in the bulk-flow model family, see i.e. [13]-[16]. In the last inertia regime of $Re_{z}^{*} \sim \mathcal{O}(1)$, the development of velocity profiles is an important feature of the flow. To the authors' knowledge, no fast (i.e. 2D) design tools have been developed for this regime, yet. The only published approaches able to incorporate such effects besides CFD are 3D methods, i.e. [17], [18].

Finally, the requirements for a unified modeling approach regarding different inertia regimes are: On the one hand, the convective terms need to be included in the momentum balances to cover arbitrary Re_{φ}^{*}. On the other hand, arbitrary velocity profiles especially including non-developed velocity profiles need to be treated in order to cover arbitrary Re_{z}^{*}.

Compatibility to Existing Knowledge

Friction at rotor and stator, respectively, is a parameter of major and universal importance for the thin film flow. Nevertheless, friction itself must be modeled differently according to the 'friction regime', i.e. laminar, hydraulically smooth, hydraulically rough and the transitional friction regimes in between. Friction modeling has been investigated in great detail in hydrodynamic lubrication research. Many publications are available that predict the hydrodynamic forces for different friction regimes, see i.e. the 'turbulence parameters' for Reynolds' differential equation by Constantinescu [11], [19] or the overview on friction factor modeling for the bulk-flow approach in [15]. Consequently, the requirement for a unified modeling approach is to be compatible to the vast knowledge accumulated in this field.

3. Clearance-Averaged Pressure Model (CAPM)

The following sections describe the unified design tool we analytically developed according to the requirements defined in the preceding chapter and which we denote 'Clearance-Averaged Pressure Model' (CAPM). Firstly, the analytic approach and the steps leading to the governing equations will be explained. Secondly, the numerical solution of the resulting system of equations is presented.

To model plain journal bearings and annular seals in a universal way, the generic geometry of a thin film flow inside a narrow annulus as illustrated in Fig. *2* a) is considered. The flow situation inside the annulus is complicated as the rotor's position might be eccentric with a time dependent relative eccentricity $\varepsilon(\tilde{t}) \coloneqq \tilde{e}(\tilde{t})/\tilde{\bar{h}}$, the rotor's axis might be inclined with a time dependent inclination $\gamma(\tilde{t})$ and the rotor's axis of symmetry might whirl around the stator's axis of symmetry with a time dependent dimensionless whirl frequency $\omega(\tilde{t}) \coloneqq \tilde{\omega}(\tilde{t})/\tilde{\Omega}$. The operational conditions of the flow are defined by the flow coefficient $\phi := \tilde{\bar{C}}_{z}/(\tilde{\Omega}\tilde{R})$, the dimensionless preswirl $\Gamma = \tilde{\Gamma}_{0}/(2\pi\tilde{\Omega}\tilde{R}^{2})$ and the circumferential Reynolds number $Re_{\varphi} \coloneqq \tilde{\Omega}\tilde{R}\tilde{\bar{h}}/\tilde{\nu}$. In fact, to assess the hydrodynamic forces on the rotor requires to predict the dimensionless pressure distribution $p \coloneqq 2\tilde{p}/(\tilde{\varrho}\tilde{\Omega}^{2}\tilde{R}^{2})$ inside the annulus.

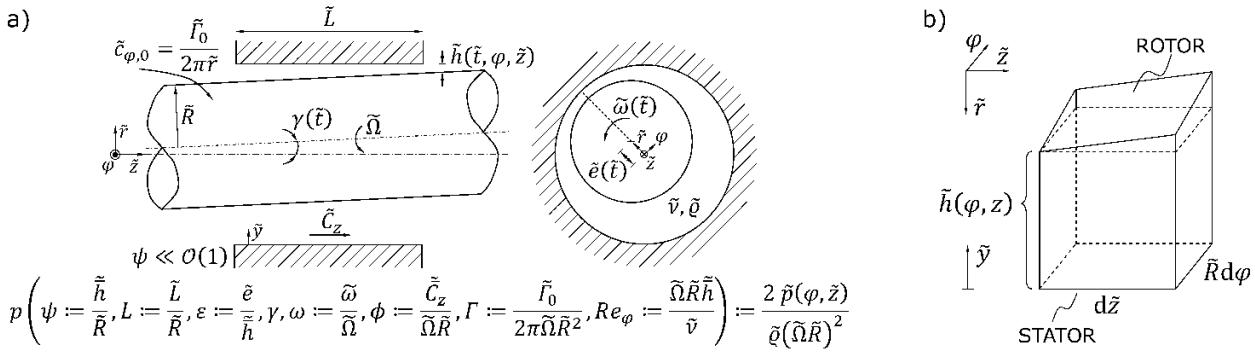

Figure 2: a) Generic journal bearing/annular seal geometry. b) Control volume inside annulus.

The modeling of the flow is carried out by means of a rotating reference frame based on cylindrical coordinates $\tilde{r}$, φ and $\tilde{z}$. The $\tilde{z}$-axis of the rotating reference frame is fixed to the axis of symmetry of the stator while the origin of the circumferential coordinate φ is fixed to the direction of the eccentricity. Especially note that in this rotating reference frame, the important case of a rotor whirling around the stator's axis of symmetry with constant eccentricity ε and constant whirl frequency ω is steady state. To evaluate the conservation equations in this rotating reference frame, the relative velocity vector $\widetilde{\vec{w}} = \tilde{c}_r\vec{e}_r + \tilde{w}_\varphi\vec{e}_\varphi + \tilde{c}_z\vec{e}_z$ is applied where $\tilde{w}_\varphi \approx \tilde{c}_\varphi - \tilde{\omega}\tilde{R}$ due to $\psi \ll \mathcal{O}(1)$.

Governing Equations

The conservation equations for mass, circumferential momentum and axial momentum are evaluated for a small control volume inside the narrow gap as illustrated in Fig. *2* b). The control volume covers the local gap height $\tilde{h}(\varphi,\tilde{z})$ entirely but is infinitesimal in circumferential and axial direction. We consider the flow inside the annulus to be incompressible with a homogeneous density field - in other words $\tilde{\varrho} = \mathrm{const.}$ - and that volume forces affect the flow only in a negligible way. A coordinate transformation to the local channel coordinate $\tilde{y} \coloneqq \tilde{R} + \tilde{\bar{h}} - \tilde{r}$ is applied, c.f. Fig. *2*. The nondimensionalization is carried out by means of the dimensionless local channel height $h(\varphi,z) \coloneqq \tilde{h}(\varphi,\tilde{z})/\tilde{\bar{h}}$, time $t \coloneqq \tilde{t}\tilde{\Omega}$, coordinates $y \coloneqq \tilde{y}/\tilde{h} = \tilde{y}/\left(h\tilde{\bar{h}}\right)$ and $z \coloneqq \tilde{z}/\tilde{L} = \tilde{z}/\left(L\tilde{R}\right)$, velocities $w_\varphi \coloneqq \tilde{w}_\varphi/\left(\tilde{\Omega}\tilde{R}\right)$ and $c_z \coloneqq \tilde{c}_z/\left(\phi\tilde{\Omega}\tilde{R}\right)$ and stresses $\tau_{i,j} \coloneqq 2\tilde{\tau}_{i,j}/\left(\tilde{\varrho}\tilde{\Omega}^2\tilde{R}^2\right)$. To ensure simplicity and efficiency of the tool to be developed, the orders of magnitude of all terms of the resulting nondimensional equations were analyzed. The analyses yield that laminar and turbulent stresses in the fluid are negligible - except those exerted by the walls and contained in $\tau_{\mathrm{Stat/Rot},\varphi/z}$ in the following. The argumentations exclusively rely on the geometrical feature $\psi \ll \mathcal{O}(1)$ of the annulus. Finally, we receive the nondimensional form of the governing equations

$$\frac{\partial h}{\partial t} + \frac{\partial}{\partial\varphi}\left(h\int_0^1 w_\varphi\,\mathrm{d}y\right) + \frac{\phi}{L}\frac{\partial}{\partial z}\left(h\int_0^1 c_z\,\mathrm{d}y\right) = 0,$$

$$h\int_0^1 \frac{\partial w_\varphi}{\partial t}\,\mathrm{d}y + h\frac{\partial\omega}{\partial t} + (1-\omega)\frac{\partial h}{\partial t} + \frac{\partial}{\partial\varphi}\left(h\int_0^1 w_\varphi^2\,\mathrm{d}y\right) + \frac{\phi}{L}\frac{\partial}{\partial z}\left(h\int_0^1 w_\varphi c_z\,\mathrm{d}y\right) = -\frac{h}{2}\frac{\partial p}{\partial\varphi} + \frac{\sum\tau_\varphi}{2\psi}, \quad (5)$$

$$h\int_0^1 \frac{\partial(\phi c_z)}{\partial t}\,\mathrm{d}y + \phi\frac{\partial}{\partial\varphi}h\int_0^1 w_\varphi c_z\,\mathrm{d}y + \frac{\phi^2}{L}\frac{\partial}{\partial z}h\int_0^1 c_z^2\,\mathrm{d}y = -\frac{h}{2L}\frac{\partial p}{\partial z} + \frac{\sum\tau_z}{2\psi}$$

where $\sum \tau_\varphi \coloneqq \tau_{\mathrm{Stat},\varphi} - \tau_{\mathrm{Rot},\varphi}$ and $\sum \tau_z \coloneqq \tau_{\mathrm{Stat},z} - \tau_{\mathrm{Rot},z}$ were used for convenience. The reader should note that in Eqn. 5, pressure is assumed to be uniform across the channel height due to Eqn. 2. Furthermore, the velocity profiles in circumferential and axial direction w_φ and c_z, respectively, are considered variable across the channel height. No further assumption on the magnitude or shape of these profiles was necessary so far. Note that all simplifying steps leading to Eqn. 5 were possible to argument with the fundamental geometrical feature of the annulus $\psi \ll \mathcal{O}(1)$.

At this point, we summarize the features and improvement of our 'Clearance-Averaged Pressure Model' (CAPM) with regard to the state of the art in hydrodynamic lubrication theory:

(i) Due to the fundamental assumption of Eqn. 2, the CAPM remains a 2D approach. Thus, it recovers the principal requirement to be a fast and efficient design tool.

(ii) The CAPM as given in Eqn. 5 is able to serve as a universal model basis for all inertia regimes as defined in chapter **2**. Convective terms on the left hand sides of the momentum equations are included and arbitrary velocity profiles including laminar profiles, turbulent profiles and also non-developed velocity profiles can be handled in an inherent way. Especially note that neglecting the convective terms recovers Reynolds' differential equation while introduction of clearance-averaged velocities instead of velocity profiles recovers the bulk-flow model.

(iii) By means of the wall shear stress modules $\sum \tau_\varphi$ and $\sum \tau_z$, the CAPM provides a clear interface to already available friction models for the different friction regimes as explained in chapter **2**.

Furthermore, due to the full transient derivation of this generalized modeling framework, the CAPM is able to calculate arbitrary rotor movements including time varying eccentricities, angles of inclination and whirl frequencies. Although it is not planned or projected yet, the adaption of extensions to Reynolds' differential equation and the bulk-flow model such as i.e. consideration of cavitation or temperature distribution inside the annulus is supposed to be straightforward.

Numerical Solution

Due to their complexity, numerical solution of the governing equations, Eqn. 5, seems appropriate. As the flow described by the CAPM is incompressible, a special methodology to calculate the pressure needs to be applied. The iterative solution is implemented in Matlab® as an explicit time stepping scheme including a pressure projection method on a staggered finite-differencing grid. The solution variables are the dimensionless pressure p and the dimensionless fluxes

$$\mathfrak{F}_\varphi \coloneqq h \int_0^1 w_\varphi \,\mathrm{d}y \quad \text{and} \quad \mathfrak{F}_z \coloneqq h \int_0^1 c_z \,\mathrm{d}y \,. \tag{6}$$

The treatment of the velocity profiles is a crucial point in the solution of Eqn. 5. In our solution algorithm, velocity profiles are considered by means of compound power law profiles

$$w_\varphi = \begin{cases} \left(W_{\varphi,\mathrm{CL}} + \omega - 1\right)\left(\dfrac{y_{\mathrm{Rot}}}{\delta_{\mathrm{Rot}}}\right)^{\frac{1}{n_\varphi}} + 1 - \omega \\ W_{\varphi,\mathrm{CL}} \\ \left(W_{\varphi,\mathrm{CL}} + \omega\right)\left(\dfrac{y}{\delta_{\mathrm{Stat}}}\right)^{\frac{1}{n_\varphi}} - \omega \end{cases}, \quad c_z = \begin{cases} C_{z,\mathrm{CL}}\left(\dfrac{y_{\mathrm{Rot}}}{\delta_{\mathrm{Rot}}}\right)^{\frac{1}{n_z}} & \text{for } 0 \le y_{\mathrm{Rot}} \le \delta_{\mathrm{Rot}} \\ C_{z,\mathrm{CL}} & \text{else} \\ C_{z,\mathrm{CL}}\left(\dfrac{y}{\delta_{\mathrm{Stat}}}\right)^{\frac{1}{n_z}} & \text{for } 0 \le y \le \delta_{\mathrm{Stat}} \end{cases} \tag{7}$$

where $y_{\mathrm{Rot}} := 1 - y$ is the local channel coordinate whose origin is located at the rotor wall, n_φ and n_z stand for the different power law exponents $n_{\mathrm{Stat},\varphi}$, $n_{\mathrm{Rot},\varphi}$, $n_{\mathrm{Stat},z}$ and $n_{\mathrm{Rot},z}$, respectively, and δ_{Stat} and δ_{Rot} stand for the different boundary layer thicknesses $\delta_{\mathrm{Stat},\varphi}$, $\delta_{\mathrm{Rot},\varphi}$, $\delta_{\mathrm{Stat},z}$ and $\delta_{\mathrm{Rot},z}$, respectively. In each time step, the centerline velocities $W_{\varphi,\mathrm{CL}}$ and $C_{z,\mathrm{CL}}$ at each position φ, z can be derived from the current flux values $\mathfrak{F}_\varphi$ and $\mathfrak{F}_z$ of Eqn. 6 by means of the velocity profiles of Eqn. 7 and the current power law exponents and boundary layer thicknesses. Based on these now completely known velocity profiles $w_\varphi(y)$ and $c_z(y)$, the convective integrals as well as the wall shear stress terms in Eqn. 5 can be evaluated by means of numerical integration.

In the present paper, we use Hirs' approach [20] to model the wall shear stresses in Eqn. 5 by means of the Fanning friction factor f as $\tilde{\tau}_{\mathrm{wall}} = f\tilde{\varrho}\tilde{C}_{\mathrm{ref}}^2/2$. We chose Hirs' model as first friction module for the CAPM because it is simple and frequently utilized for annular seals. In this model, the Fanning friction factor is determined according to $f = m_f Re_{\mathrm{ref}}^{n_f}$ that represents hydraulically smooth flow well for $n_f \approx -0.25$. The numerical value of the second constant m_f varies a lot in literature. Hirs assumed his model to be valid even for different types of flows if the reference relative velocity $\tilde{C}_{\mathrm{ref}}$ (and $Re_{\mathrm{ref}} := 2\tilde{C}_{\mathrm{ref}}\bar{\tilde{h}}/\tilde{\nu}$) is chosen properly. For this first version of the CAPM, we interpret $\tilde{C}_{\mathrm{ref}}$ as the velocity relative to the adjacent wall averaged over the respective boundary layer thickness.

After this explicit part of the time stepping scheme is completed, the pressure projection method is applied. A pressure distribution is determined that enforces the flux fields of Eqn. 6 to satisfy the continuity equation by means of the solution of a Poisson equation for the pressure corrections. Finally, the flux fields are corrected by means of this pressure correction field to complete the time step. The described procedure corresponds to the SIMPLE algorithm, see i.e. [21].

The solution procedure for the flow variables $\mathfrak{F}_\varphi$, $\mathfrak{F}_z$ and p is now complete. During the solution steps described above, the 8 boundary layer variables n and δ were assumed to be known. Of course, a special model for the velocity profile development in each time step needs to be coupled with the flow solver in order to fully recover the flow behavior of inertia regime $Re_z^* \sim \mathcal{O}(1)$. We think that the integral or Pohlhausen's method might be an efficient analytic base for that purpose, see i.e. [22]. This method has recently been adopted by our colleagues to describe the coupled circumferential and axial boundary layer development at the inlet of a rotating pipe [23], [24]. The integration of such methods into the solution algorithm is matter of our future work. For the present paper, we set the power law exponents $n := \mathrm{const}$ and the boundary layer thicknesses $\delta := h/2$.

4. Results and Comparison to CFD

Purpose of the following chapter is to apply the CAPM to test cases with geometrical and operational conditions representing typical plain annular seal applications. In this paper, we restrict our considerations to cases that are steady in respect to the rotating reference frame. However, the reader should note that due to the utilization of the rotating reference frame, the steady

CAPM still includes both static eccentricities as well as whirling rotor configurations with $\omega = \mathrm{const}$. The test cases considered are characterized by the relative clearance $\psi = 4\,‰$ and the dimensionless length $L = 1$. The rotor is positioned at a static eccentricity with $\varepsilon = 0.3$ and $\omega = 0$ where the axes of symmetry of rotor and stator remain parallel, i.e. $\gamma = 0$. The operating conditions are characterized by the circumferential Reynolds number $Re_\varphi = 5350$ yielding $Re_\varphi^* = 21.4$ and three flow numbers $\phi = 0.3$, 0.6 and 1.3 yielding $Re_z^* = 7$, 13 and 28, respectively. Furthermore, the dimensionless preswirl Γ is varied in 4 steps in the range $0 \leq \Gamma \leq 1.35$ for each flow number. As the flow inside the annulus is considered turbulent, power law exponents $n_\varphi = 3$ and $n_z = 6.5$ are applied to calculate all integrals in Eqn. 5 and during the determination of $\tilde{C}_{\mathrm{ref}}$. For all numerical calculations presented in this paper, fixed values for the fluxes at the annulus' inlet $\mathfrak{F}_{\varphi,0}$ and $\mathfrak{F}_{z,0}$ and a fixed mean pressure $\left(\sum_i \Delta\varphi_i p_{i,1}\right)/\left(\sum_i \Delta\varphi_i\right) = 0$ at the outlet were applied as boundary conditions.

In a first step of this exemplary application, a grid study was carried out for the spatial discretization of the staggered finite-differencing grid utilized for numerical solution of the CAPM. This study showed that a resolution of 25 x 25 points is sufficient to achieve the required accuracy: Refinement of the finite-differencing grid to a resolution of 49 x 49 points increases the computational time significantly but changes the predicted hydrodynamic radial and tangential forces F_r and F_φ only by approximately $3\,\%$ or less. In contrast to that, a finite-differencing grid with reduced resolution of 13 x 13 points predicts forces that differ by approximately $10\,\%$ from the results of the 25 x 25 grid.

In the following, the results of the CAPM are compared to results of CFD simulations to assess their accuracy. The CFD simulations were carried out with ANSYS® Fluent and utilization of a Reynolds stress turbulence model (RSM). The CFD model was a three dimensional model consisting of 26 cells in radial, 1596 cells in circumferential and 263 cells in axial direction. A grid study for the most critical operating point with $\phi = 1.3$ and $\Gamma = 1.35$ showed that this spatial discretization with 10.9 million cells yielding values of $y^+ \approx 3$ at all walls is necessary to reach the required accuracy. A turbulence model study including additional simulations by means of the realizable $k-\varepsilon$ model and the $k-\omega-SST$ model showed that all turbulence models predict nearly equivalent pressure distributions inside the annulus. Furthermore, we checked and assured that the pressure distributions predicted by the RSM do not depend on the inlet turbulence intensity which we varied in the range $1\,\% \leq Tu \leq 10\,\%$. Finally, we fixed $Tu = 4\,\%$ at the inlet for the parameter study.

Typical computing times for single cases are in the range of 5 h on 16 CPUs (3.3 GHz) for the CFD simulations and in the range of 6 min on a single CPU (2.3 GHz) for the CAPM. After this time, the forces predicted by the CAPM calculation reached the final converged state within a tolerance of less than $1\,\%$. The reader should note that no optimization steps to the solution procedure of the CAPM have been carried out so far. First ideas for such measures are given in the outlook.

As the numerical value of m_f in Hirs' friction model is unknown, a calibration of the CAPM's friction representation must be carried out. This is realized in terms of a calibration of m_f in the following way: A concentric rotor (axisymmetric) case was calculated by means of both CFD and CAPM. The axial pressure gradient predicted by both approaches was matched by means of an adjustment of m_f for the CAPM. It is known that the resistance coefficient $\lambda := 4f$ of an annulus with inner rotating cylinder is a function of the flow number, i.e. $\lambda(\phi)$ [25]. Consequently, it was necessary to apply the calibration of m_f for all three flow numbers separately. However, the reader should note that the calibrations have been carried out only once for each value of ϕ and that this calibration was done for the case of a concentric rotor. Afterwards, the values

$m_f(\phi = 0.3) \approx 0.122$, $m_f(0.6) \approx 0.114$ and $m_f(1.3) \approx 0.109$ were kept constant for the eccentric rotor calculations with varying preswirl.

In the following, the results of the parameter study with eccentric rotor as defined at the beginning of the chapter are presented. The nondimensional hydrodynamic forces $F \coloneqq 2\tilde{F}/\left(\tilde{\varrho}\tilde{\Omega}^2\tilde{R}^3\tilde{L}\right)$ in radial (direction of eccentricity) and tangential (orthogonal to direction of eccentricity) direction F_r and F_φ calculated by means of CFD and the CAPM are shown in Fig. *3* a). In case of the nondimensional radial force, CAPM and CFD predictions agree well. The differences are smaller than $10\,\%$ for all operating points considered. In case of the nondimensional tangential force, the results are not that clear. Two characteristic aspects can be observed: (i) The tangential forces predicted by CAPM and CFD agree in an acceptable way for the smallest flow number $\phi = 0.3$. The differences are smaller than $30\,\%$ for all values of preswirl considered and the tendency $F_\varphi(\Gamma)$ is predicted correctly for this flow number. (ii) The tangential forces agree well for the value of preswirl $\Gamma = 0.45$ independent of the flow number. The differences are smaller than $20\,\%$ for all values of flow number but the CAPM prediction overshoots the CFD prediction for $\phi = 0.3$ and undershoots the CFD prediction for $\phi = 1.3$, respectively. For all other operating points, significant differences between the tangential forces predicted by the CAPM and CFD can be observed.

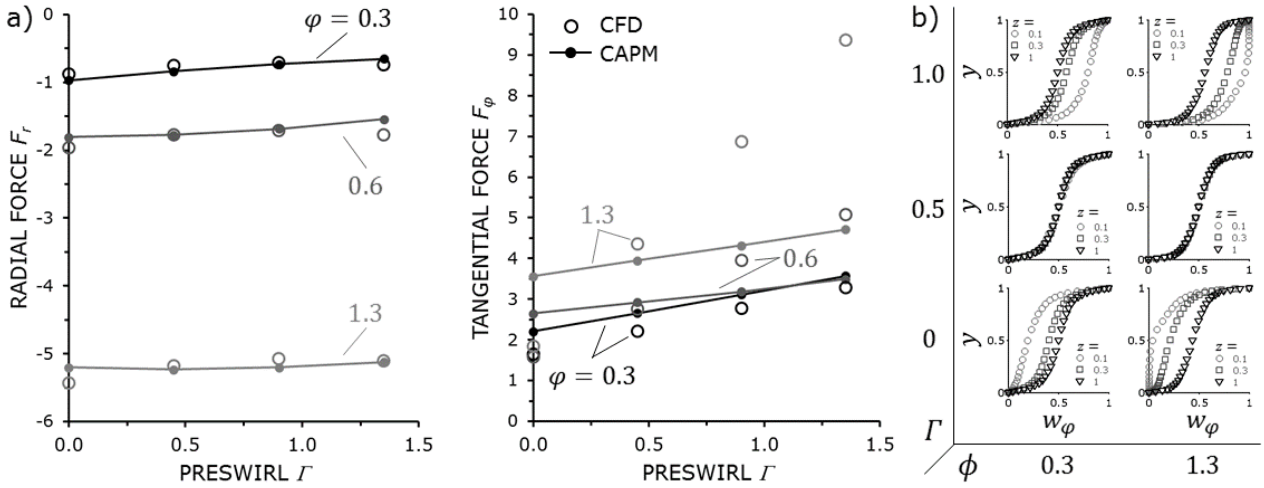

Figure 3: a) Hydrodynamic forces predicted by CFD and CAPM. b) Circumferential velocity profile development in a concentric rotor configuration for different operational parameters predicted by CFD.

We think that the differences in the prediction of the tangential forces can be explained by means of the missing treatment of velocity profile development in our CAPM up to now. In Fig. *3* b), the circumferential velocity profiles predicted by CFD at different axial positions z inside the annulus are shown for calculations with concentric rotor and different operational parameters ϕ and Γ. Again, we observe the two characteristics we already saw in Fig. *3* a): (i) In case of small flow number, i.e. $\phi = 0.3$, the circumferential velocity profile develops within a short axial distance. At $z = 0.3$, $w_\varphi(y)$ nearly reached its fully developed state typically known from turbulent Couette flow. Whether the preswirl is $\Gamma < 0.5$ or $\Gamma > 0.5$ only determines if the flow is accelerated or decelerated in circumferential direction, respectively. In contrast to that, $w_\varphi(y)$ still is far from being fully developed at $z = 0.3$ in case of the high flow number $\phi = 1.3$. Furthermore, we can explicitly observe that in case of $\Gamma = 0$, $w_\varphi(y)$ begins to develop from the rotor at $y = 1$ and that the boundary layer thickness $\delta_{\mathrm{Rot},\varphi}$ nearly covers the entire channel height at small axial positions z. In case of $\Gamma = 1$, on the contrary, $w_\varphi(y)$ begins to develop from the stator at $y = 0$ and now the boundary layer thickness $\delta_{\mathrm{Stat},\varphi}$ nearly covers the entire channel

height for small z. (ii) In case of preswirl $\Gamma = 0.5$, $w_\varphi(y)$ starts developing from both rotor and stator at the same time. Consequently, the axial distance necessary to reach a fully developed state is much smaller than for $\Gamma \neq 0.5$. In contrast to the circumferential velocity profile $w_\varphi(y)$, we observed that the axial velocity profile $c_z(y)$ reaches a fully developed state at much smaller axial positions for all operating points considered in Fig. *3* b).

5. Conclusion and Outlook

Finally, we conclude that the assumption of fully developed velocity profiles as it is currently implemented in our CAPM is appropriate only for special cases, i.e. small flow numbers or preswirl $\Gamma = 0.5$. The observations indicate that the axial film Reynolds number Re_z^* as defined in Eqn. 4 really serves as a measure for the relevance of velocity profile development in the thin film flow. In case of $Re_z^* = 7$ ($\phi = 0.3$), the development of $w_\varphi(y)$ can be observed but it does not seem to influence the prediction of hydrodynamic forces significantly. In contrast to that, for $Re_z^* = 28$ ($\phi = 1.3$), the region of velocity profile development covers a remarkable portion of the annulus and the predicted hydrodynamic forces are significantly influenced as consequence. The reader should note that in case of an eccentric rotor configuration, the influence of inertia and velocity profile development, respectively, is expected to be higher.

Hence, the incorporation of a model for the velocity profile development in our CAPM is matter of our future work. In addition, we think that the solution time can be reduced remarkably by introducing a more implicit treatment of the convective terms during the solution of Eqn. 5. Perspectively, flow models for the inlet and exit of the annulus are required especially for calculation of annular seals and hydrostatic journal bearings. Finally, we plan experiments to validate both our CAPM as well as the CFD calculations we use for comparison. The corresponding test bench with magnetically levitated rotor is under construction at the institute right now.

Acknowledgment

We would like to thank for the computing time grant we received from the Lichtenberg cluster at TU Darmstadt. Without this CPU time, the present investigations would not have been possible.

References

[1] Brennen, C. E.: Hydrodynamics of Pumps, Oxford University Press, 1994.
[2] Amoser, M.: Strömungsfelder und Radikalkräfte in Labyrinthdichtungen hydraulischer Strömungsmaschinen, PhD thesis, ETH Zürich, Switzerland, 1995.
[3] Szeri, A. Z.: Fluid film lubrication: Theory and design, Cambridge Univ. Press, 2005.
[4] Knopf, E.: Identifikation der Dynamik turbulenter Gleitlager mit aktiven Magnetlagern, PhD thesis, Technische Universität Darmstadt, Germany, Shaker, 2001.
[5] Childs, D.: Turbomachinery Rotordynamics: Phenomena, Modeling and Analysis, USA: John Wiley & Sons, 1993.
[6] Florjancic, S.: Annular seals of high energy centrifugal pumps, PhD thesis, ETH Zürich, 1990.
[7] Kahlert, W.: Der Einfluss der Trägheitskräfte bei der hydrodynamischen Schmiermitteltheorie, Ingenieur-Archiv, 16(5-6), pp. 321–342, 1948.
[8] Osterle, F.; Saibel, E.: On the effect of lubricant inertia in hydrodynamic lubrication, Journal of Applied Mathematics and Physics, ZAMP, 6, p. 334, 1955.
[9] King, K. F.; Taylor, C. M.: An estimation of the effect of fluid inertia on the performance of the plane inclined slider thrust bearing with particular regard to turbulent lubrication, ASME, Transactions, Series F-Journal of Lubrication Technology, 99, pp. 129–135, 1977.
[10] Launder, B. E.; Leschziner, M.: Flow in finite-width thrust bearings including inertial effects I & II, Journal of Lubrication Technology, 100(3), p. 330, 1978.
[11] Constantinescu, V.; Galetuse, S.: Operating characteristics of journal bearings in turbulent inertial flow, Journal of Tribology, 104(2), pp. 173–179, 1982.
[12] Elrod, H. G.; Anwar, I.; Colsher, R.: Transient lubricating films with inertia, Journal of Lubrication Technology, 105(3), p. 369, 1983.
[13] Childs, D. W.: Dynamic analysis of turbulent annular seals based on Hirs' lubrication equation, Journal of

Lubrication Technology, 105(3), p. 429, 1983.
[14] San Andres, L.: Turbulent hybrid bearings with fluid inertia effects, Journal of Tribology, 112(4), p. 699, 1990.
[15] Zirkelback, N.; San Andres, L.: Bulk-Flow Model for the Transition to Turbulence Regime in Annular Pressure Seals, Tribology Transactions, 39(4), p. 835, 1996.
[16] San Andres, L.; Childs, D.: Angled injection - hydrostatic bearings analysis and comparison to test results, Journal of Tribology, 119(1), p. 179, 1997.
[17] Shyu, S.-H.; Jeng, Y.-R.: An efficient general fluid-film lubrication model for plane slider bearings, Tribology Transactions, 45(2), pp. 161–168, 2002.
[18] Kyle, J. P.; Terrell, E. J.: Application of smoothed particle hydrodynamics to full-film lubrication, Journal of Tribology, 135(4), p. 041705., 2013.
[19] Constantinescu, V.N.: Basic Relationships in Turbulent Lubrication and Their Extension to Include Thermal Effects, Journal of Lubrication Technology, Vol. 95, S. 147 – 154, 1973.
[20] Hirs, G.: A bulk-flow theory for turbulence in lubricant films, Journal of Tribology, 95(2), pp. 137–145, 1973.
[21] van Doormaal, J. P.: Raithby, G. D.: Enhancements of the SIMPLE method for predicting incompressible fluid flows, Numerical Heat Transfer, 7(2), pp. 147–163, 1984.
[22] Schlichting, H.: Boundary-Layer Theory, McGraw Hill, 1970.
[23] Stapp, D.; Pelz, P.: Evolution of swirl boundary layer and wall stall at part load - a generic experiment, Proceedings of ASME Turbo Expo GT2014–26235, 2014.
[24] Stapp, D.: Experimentelle und analytische Untersuchung zur Drallgrenzschicht, PhD thesis, TU Darmstadt, Germany, 2015
[25] Yamada, Y.: Resistance of a Flow through an Annulus with an Inner Rotating Cylinder, Bulletin of the JSME, 5(18), 1962.